

Supplementary Material

Gd-Induced Electronic Structure Engineering of NiFe-Layered Double Hydroxide for Efficient Oxygen Evolution

Meng Li,^{‡a} Hao Li,^{‡c} Xuechun Jiang,^a Mengqi Jiang,^a Xun Zhan,^d Gengtao Fu,^{*a,b} Jong-Min Lee,^{*b} and Yawen Tang^{*a}

^a Jiangsu Key Laboratory of New Power Batteries, Jiangsu Collaborative Innovation Center of Biomedical Functional Materials, School of Chemistry and Materials Science, Nanjing Normal University, Nanjing, 210023, PR China.
Email: tangyawen@njnu.edu.cn (Y. Tang)

^b School of Chemical and Biomedical Engineering, Nanyang Technology University, 637459, Singapore
Email: gengtaofu@gmail.com (G. Fu); jmlee@ntu.edu.sg (J-M. Lee)

^c Department of Physics, Technical University of Denmark, 2800 Kongens Lyngby, Denmark

^d Electron Microscopy Center, Indiana University, 800 E. Kirkwood Ave. Bloomington, IN 47405, USA

[#] M. Li and H. Li contributed equally to this work

Experimental

Reagents and chemicals

Nickel nitrate hexahydrate ($\text{Ni}(\text{NO}_3)_2 \cdot 6\text{H}_2\text{O}$) was purchased from Shanghai Second Reagent Factory (Shanghai, China), Ltd. Gadolinium nitrate hexahydrate ($\text{Gd}(\text{NO}_3)_3 \cdot 6\text{H}_2\text{O}$) and iron (III) nitrate nonahydrate ($\text{Fe}(\text{NO}_3)_3 \cdot 9\text{H}_2\text{O}$) were purchased from Yuanye Biotechnology Co. Ltd. (Shanghai, China). Ammonium fluoride (NH_4F) and urea ($\text{CO}(\text{NH}_2)_2$) was purchased from Guangzhou Jinhuada Chemical Regent Co. Ltd. (Guangzhou, China). Commercial ruthenium(IV) oxide was purchased from Shanghai D&B Biological Science and Technology Co. Ltd. (Shanghai, China). All reagents and chemicals were used without further purification.

Synthesis of Gd-NiFe-LDH@CC and NiFe-LDH@CC

The Gd-NiFe-LDH@CC and NiFe-LDH@CC were prepared by a facile one-step hydrothermal method. For the synthesis of NiFe-LDH@CC, 2.5 mmol NH_4F and 6 mmol $\text{CO}(\text{NH}_2)_2$ were dissolved in 20 ml deionized water under continuous ultrasonic dissolving and magnetic stirring for several minutes. Then, 10 ml 1.2 M mixed aqueous solution of $\text{Ni}(\text{NO}_3)_2$ and $\text{Fe}(\text{NO}_3)_3$ (labeled as solution A, and the molar ratio of Ni:Fe is 3:1) was added to the reactor. After stirring for 2 min, the solution was transferred to a Teflon-lined steel autoclave, while a piece of 2*4 cm² carbon cloth was put into the reactor vertically, followed by continuous stirring for 15 minutes. The autoclave was then heated in an oven at 120 °C for 12h. The observed carbon cloth was rinsed with deionized water for several times and dried at 80 °C overnight.

The Gd-NiFe-LDH@CC were synthesized with the similar method except that $\text{Gd}(\text{NO}_3)_3$ was introduced into the solution A. In order to investigate the influence of Gd content in LDH, Gd-NiFe-LDH@CC-1%, Gd-NiFe-LDH@CC-2.5% and Gd-NiFe-LDH@CC-5% were synthesized by controlling the molar content of $\text{Gd}(\text{NO}_3)_3$ to 1%, 2.5% and 5% in solution A, respectively.

Electrochemical Measurements

All the electrochemical measurements were executed by a typical three-electrode system on CHI 760E electrochemical analyzer (Shanghai Chenchua Co.). In a typical three-electrode system, a catalysts-modified carbon cloth (CC, 1*2 cm²) was employed as working electrode, while a carbon rod and a saturated calomel electrode (SCE) were used as the auxiliary electrode and the reference electrode, respectively. The active area of the carbon cloth in contact with the electrolyte is 1*1 cm². All of the electrochemical tests were operated in O₂-saturated 1 M KOH electrolyte. The LSV curves were measured at a sweep rate of 5 mV s⁻¹. The potentials in this manuscript were

converted to the reversible hydrogen electrode (RHE) by following equation: $E_{\text{RHE}} = E_{\text{SCE}} + 0.0592 \cdot \text{pH} + 0.242$. The electrochemical impedance spectroscopy was carried out in a frequency range from 0.01 Hz to 100 kHz at 1.45 V vs. RHE.

Characterization

The crystal structure information of the as-fabricated samples was measured by X-ray powder diffraction (XRD) on a D/max-rC X-ray diffractometer (Cu K α radiation, $\lambda = 1.5406 \text{ \AA}$). TEM and HRTEM images were captured from JEOL JEM-2100F TEM/STEM (accelerating voltage of 200 kV). Elemental mapping images, electron energy dispersive spectroscopy (EDS) measurements and HAADF-STEM images with corresponding line scanning profiles were performed on a FEI Tecnai G2 F20 microscope, an accessory built on the JEOL JEM-2100F. SEM images were acquired by JEOL JSM7500F. All XPS data were recorded on Thermo VG Scientific ESCALAB 250 spectrometer (Al K α radiator). ESR data were recorded on Bruker A300 at 77K.

Computational Methods

Density functional theory with spin-polarization, Hubbard-U corrections (DFT+U), and Van der Waals corrections (DFT+D3)^[1] were considered for all of the calculations in this study, using the Vienna *Ab initio* Simulation Package. The $U_{\text{eff}}(U-J)$ values for Fe and Ni were set as 5.3 and 6.2 eV, respectively. The generalized gradient approximation method was used to describe electron correlation with the functional developed by Perdew, Burke, and Ernzerhof.^[2] The valence electrons were described by the Kohn–Sham wave functions being expanded in a plane wave basis set.^[3] The kinetic cutoff for all calculations were set as 400 eV. The force convergence was defined when all of the forces on each atom became lower than 0.05 eV per \AA . The Brillouin zone was sampled with a $(3 \times 3 \times 1)$ k -point mesh, using the Monkhorst-Pack method.^[4] The surface Pourbaix diagrams were calculated using the method described in Ref.^[5]. The total energy of O₂, H₂O, and H₂ were calculated in vacuum with spin-polarization. The computational hydrogen electrode (CHE) method was applied for the free energy calculations,^[6] using half of the electronic energy of a H₂ molecule in vacuum to represent the electronic energy of a proton-electron pair. Previous studies have shown that the OER mechanism proposed by Man *et al.*^[7] with the CHE method leads to good agreement with the experimental overpotentials of OER on hydroxides.^[8] The NiFe LDH structures were obtained from the *MaterialsProject* database.^[9] Bulk relaxations were performed before the surfaces were cut. The calculations of OER free energy diagram were considered at a two-layer NiFe LDH surface. The entropic and zero-point energy correction values were obtained from Ref.^[10]

Figures and Captions

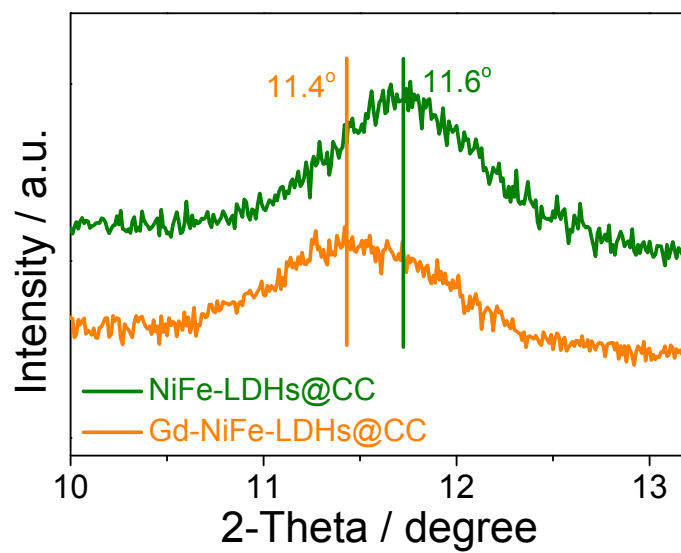


Figure S1. XRD pattern of NiFe-LDH@CC and Gd-NiFe-LDH@CC.

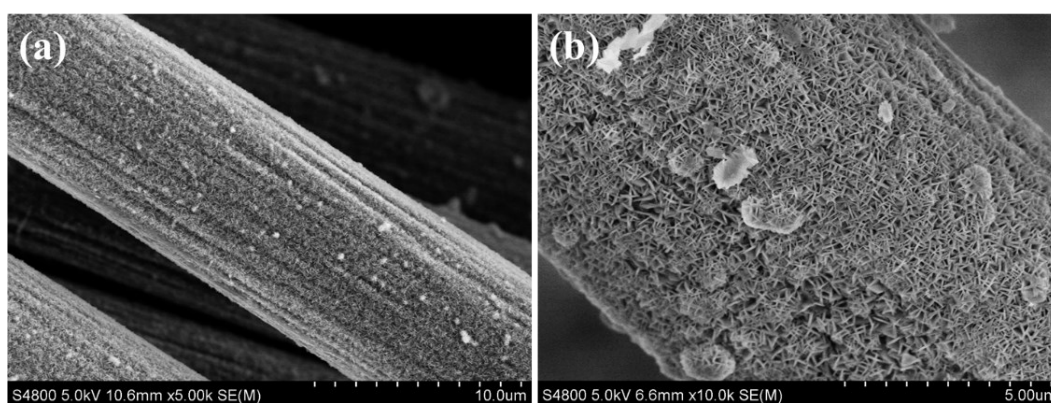


Figure S2. SEM images of Gd-NiFe-LDH@CC at different magnifications.

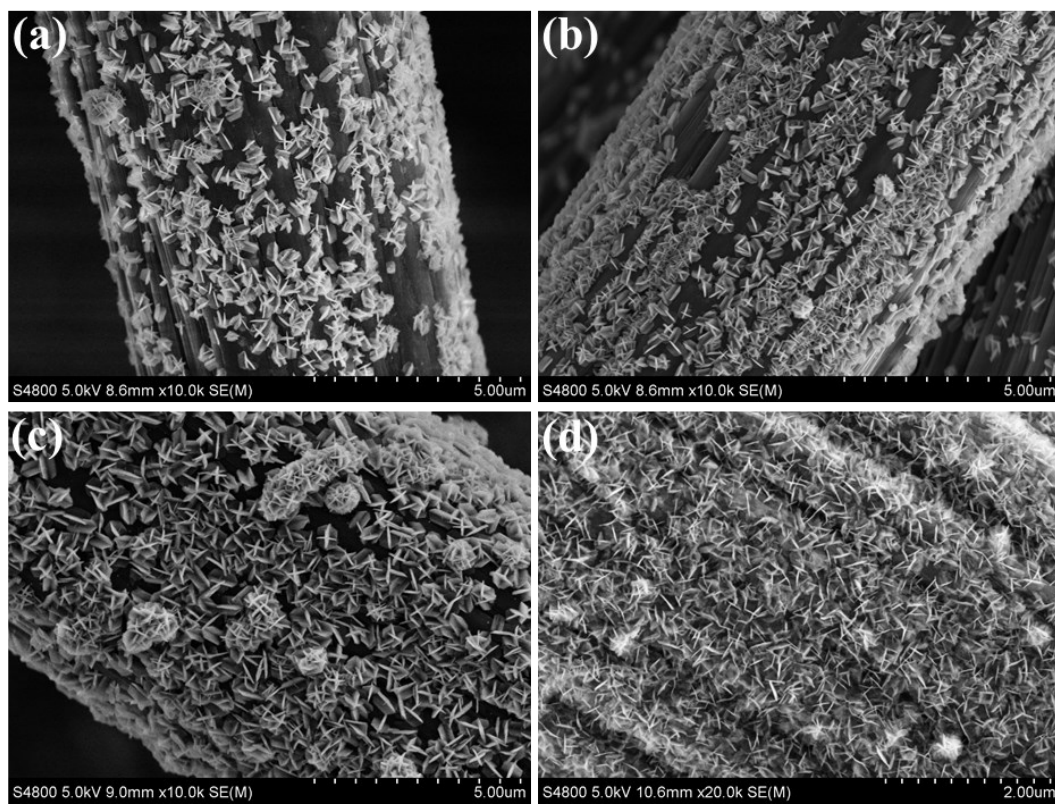


Figure S3. SEM images of Gd-NiFe-LDH@CC at reaction time of (a) 3h, (b) 6h, (c) 9h and (d) 12h.

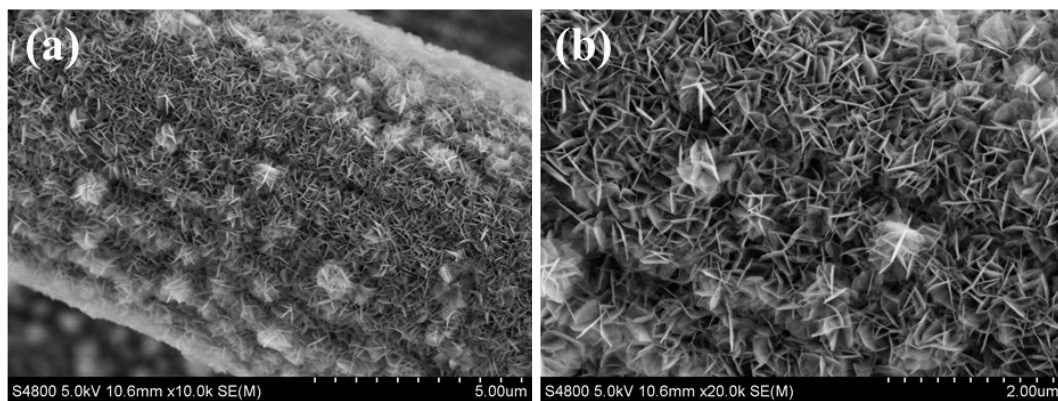


Figure S4. (a-b) SEM images of NiFe-LDH@CC at different magnifications.

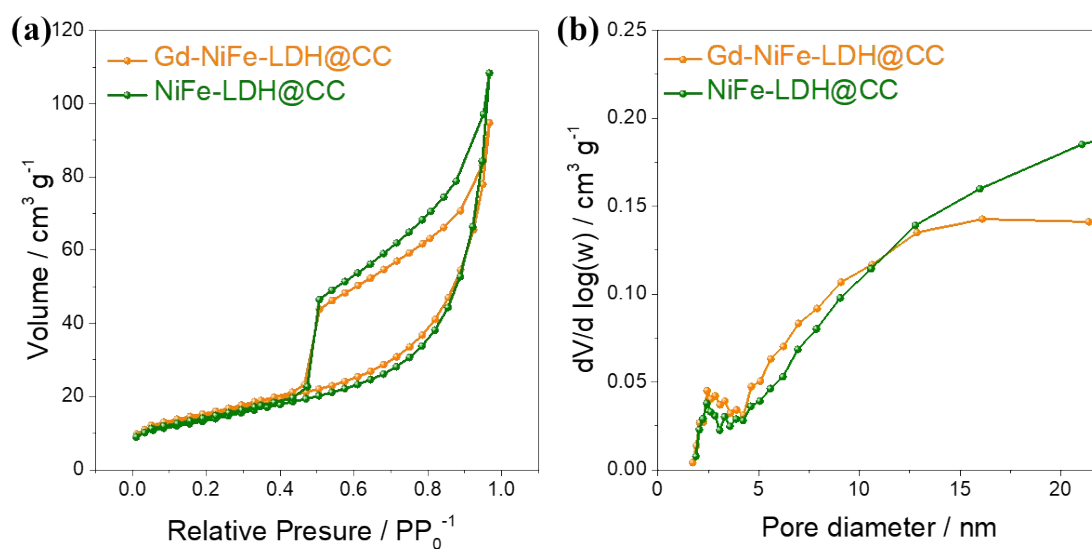


Figure S5. (a) N_2 adsorption–desorption isotherms and (b) corresponding pore size distribution curves of Gd-NiFe-LDH@CC and NiFe-LDH@CC.

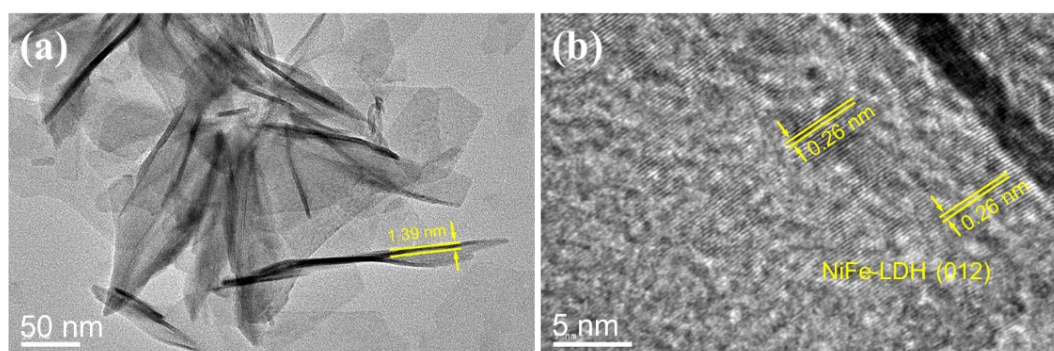


Figure S6. TEM images of Gd-NiFe-LDH@CC at different magnifications.

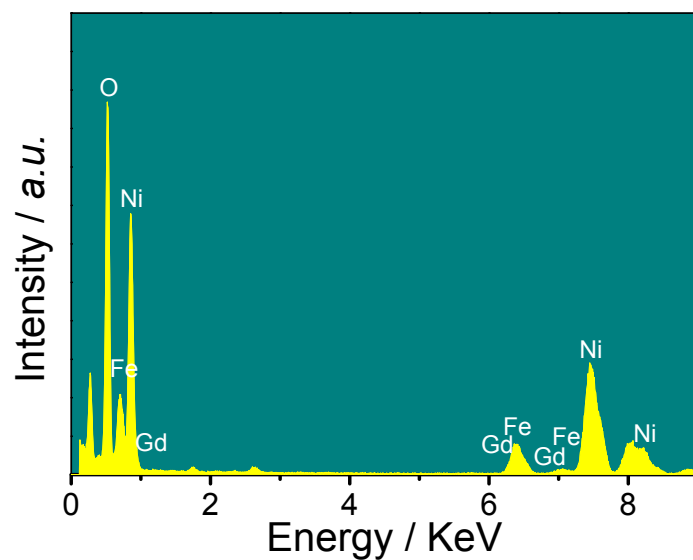


Figure S7. EDX spectrum of Gd-NiFe-LDH@CC.

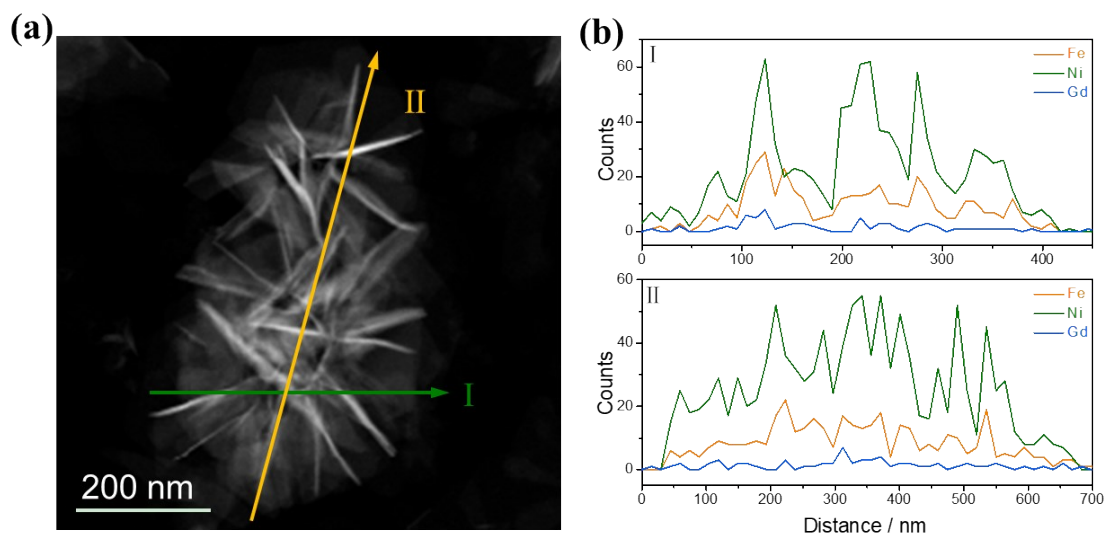


Figure S8. (a-b) STEM images spectrum and corresponding line scanning profiles of Gd-NiFe-LDH@CC.

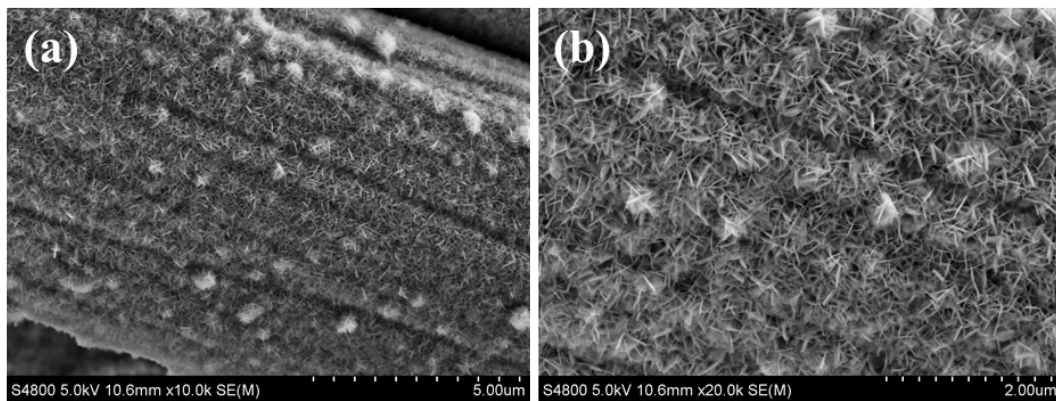


Figure S9. (a-b) SEM images of Gd-NiFe-LDH@CC-1% at different magnifications.

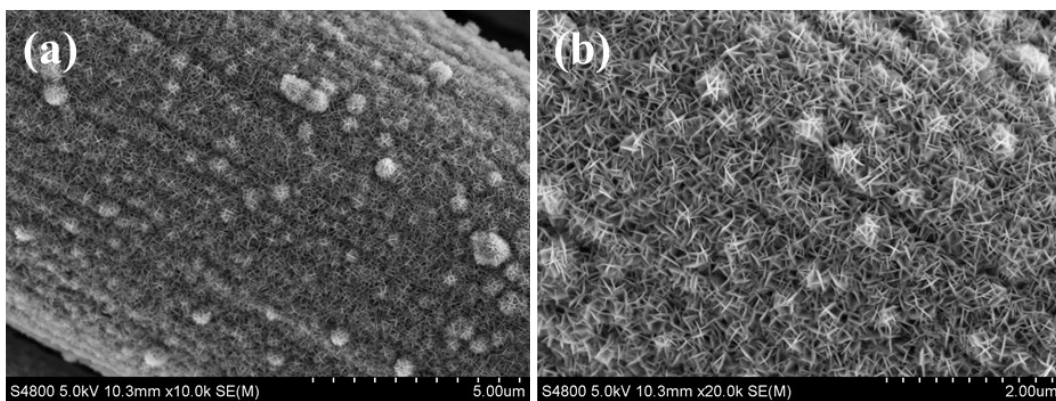


Figure S10. (a-b) SEM images of Gd-NiFe-LDH@CC-5% at different magnifications.

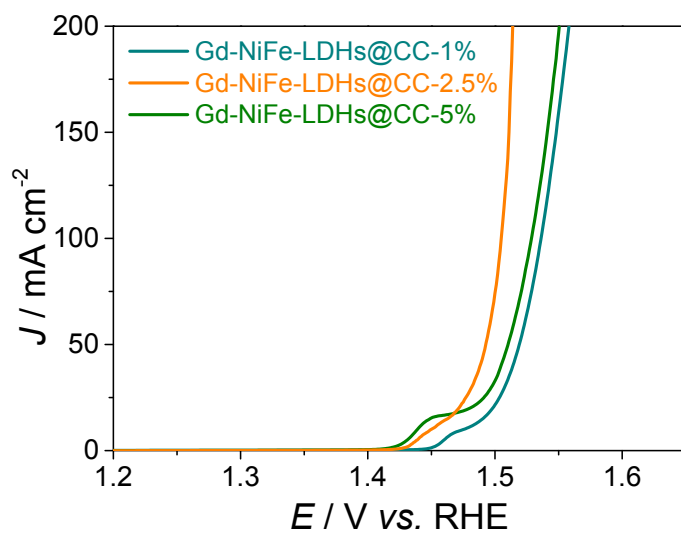


Figure S11. Comparison of OER performance of different samples in 1 M KOH solution.

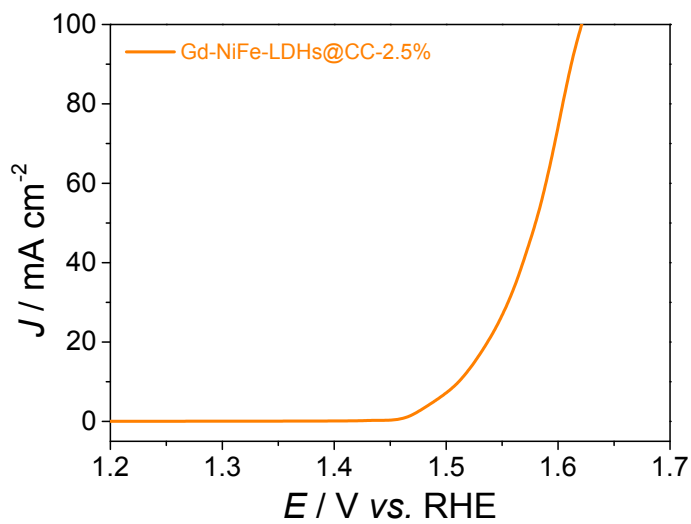


Figure S12. OER performance of Gd-NiFe-LDH@CC in 0.1 M KOH solution.

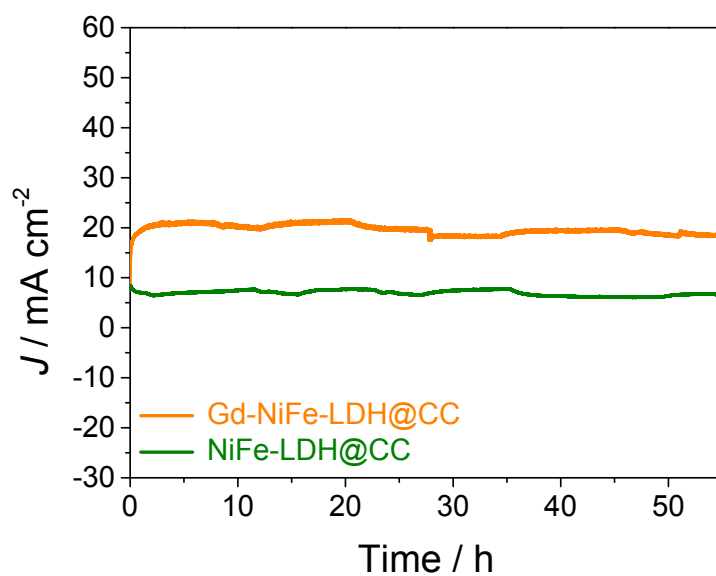


Figure S13. The chronopotentiometry curves of Gd-NiFe-LDH@CC and NiFe-LDH@CC at 1.47 V.

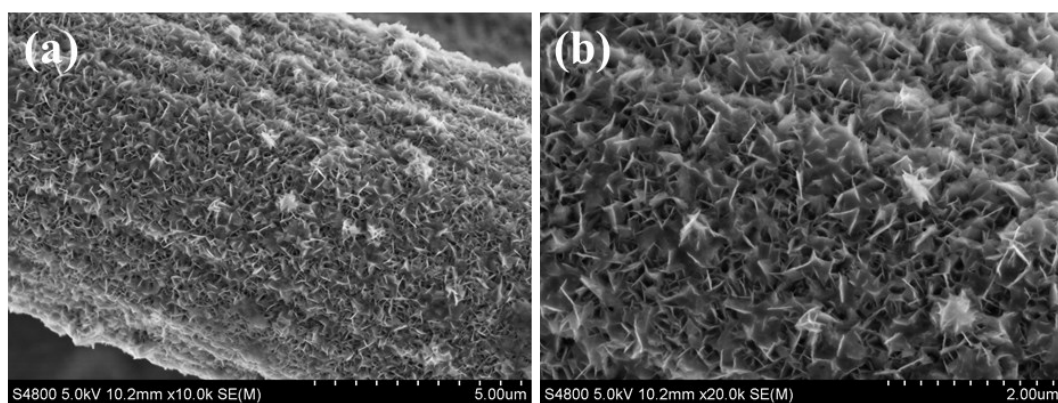


Figure S14. (a-b) SEM images at different magnifications of Gd-NiFe-LDH@CC after stability test.

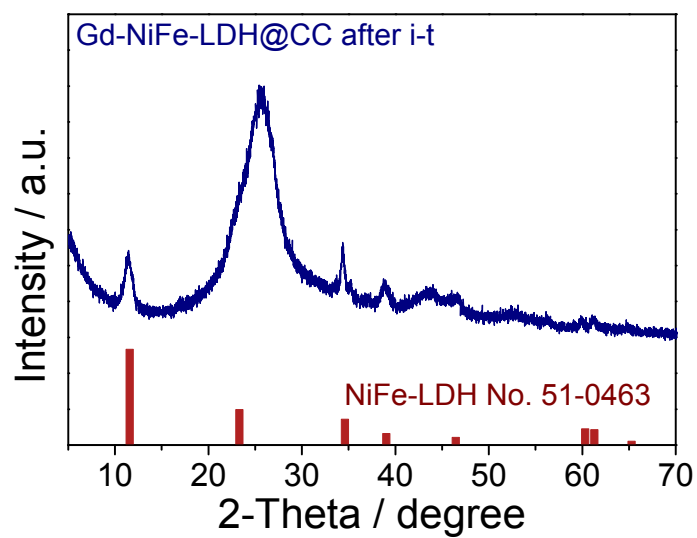


Figure 15. XRD pattern of Gd-NiFe-LDH@CC after stability test.

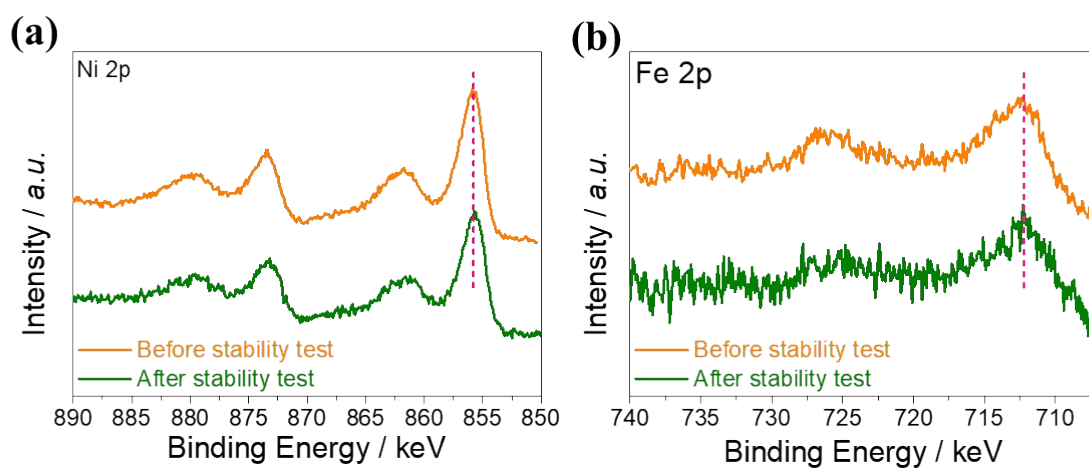


Figure S16. (a) Ni 2p and (f) Fe 2p XPS spectra of Gd-NiFe-LDH@CC before and after stability test.

Faradic efficiency test device



Figure S17. Faradic efficiency test device.

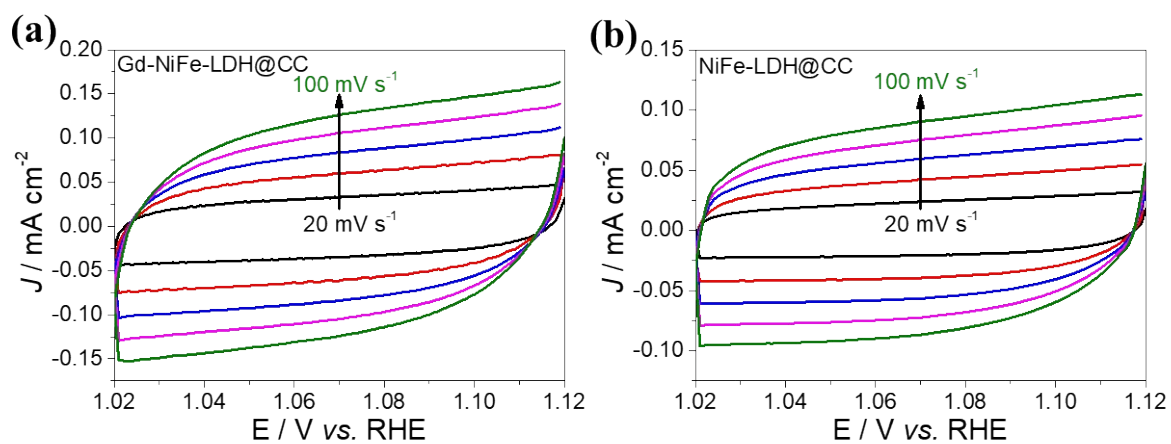


Figure S18. CVs at different sweeping rates from 20 mV s^{-1} to 100 mV s^{-1} (a) Gd-NiFe-LDH@CC; (b) NiFe-LDH@CC.

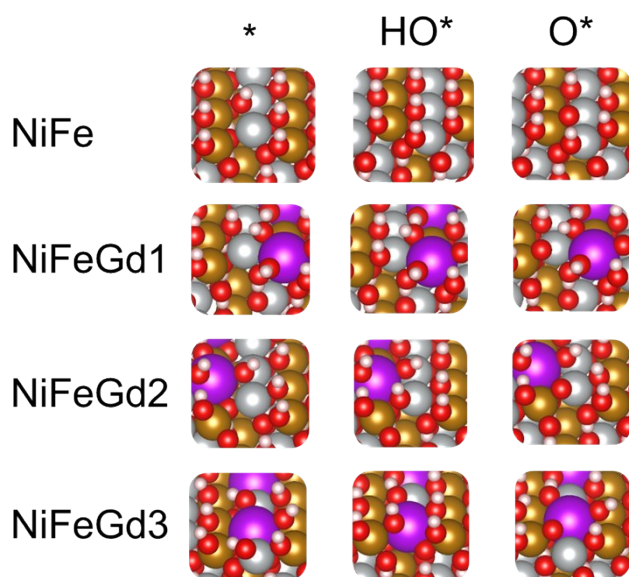


Figure S19. DFT-optimized geometries of the bare surfaces and the surfaces with adsorbed HO* and O*. Pink, red, grey, brown, and purple spheres represent H, O, Ni, Fe, and Gd, respectively.

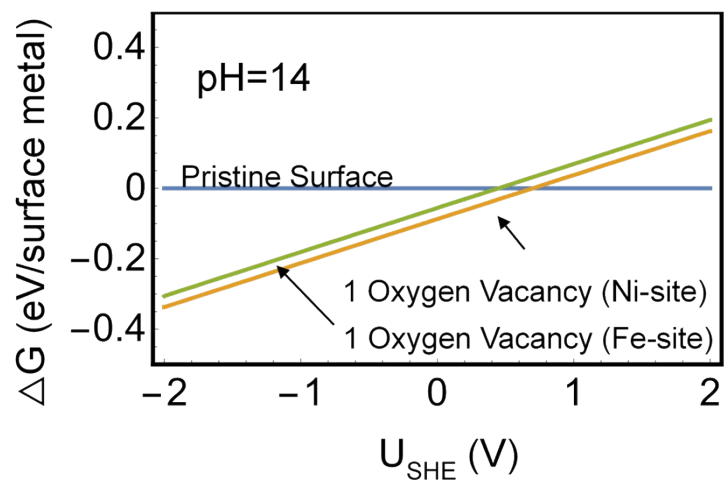


Figure S20. Calculated surface Pourbaix diagram on NiFe LDH, with pH=14. Since a more negative free energy indicates a more favorable surface states, this indicates that formation of oxygen vacancy on a Ni-site is thermodynamically favorable under OER potentials.

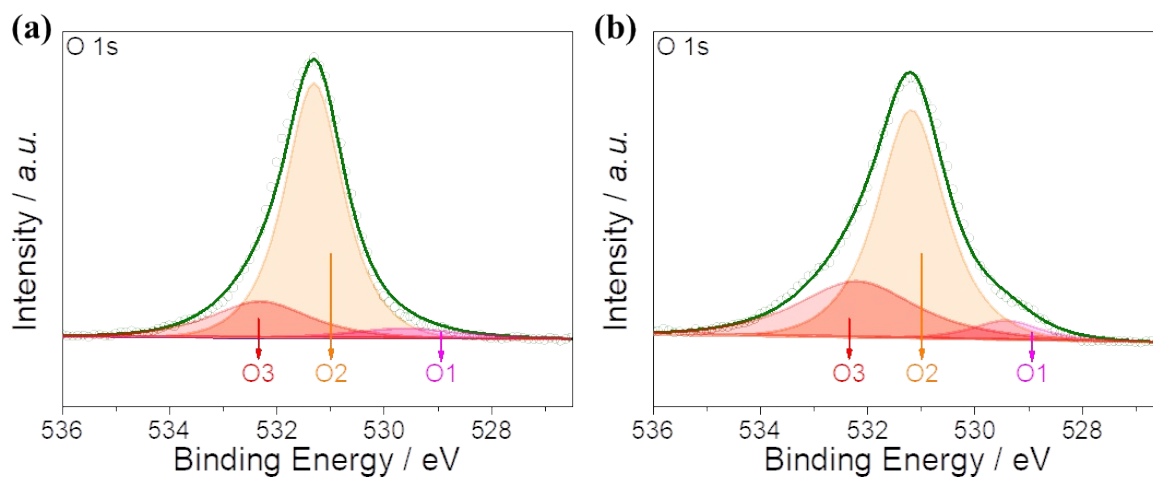


Figure S21. O1s XPS spectrum of Gd-NiFe-LDH@CC before and after OER measurement.

Table S1. Elements molar ratio in Gd-NiFe-LDH@CC-1%, Gd-NiFe-LDH@CC-2.5% and Gd-NiFe-LDH@CC-5%.

Samples	Ni content	Fe content	Gd content
Gd-NiFe-LDH@CC-1%	74.92 %	23.99 %	1.09 %
Gd-NiFe-LDH@CC-2.5%	72.97 %	24.25 %	2.78 %
Gd-NiFe-LDH@CC-5%	70.42 %	24.05 %	5.53 %

Table S2. Comparison of OER activity of Gd-NiFe-LDH@CC with other catalysts reported.

Catalysts	η_j / mV 10 mA cm ⁻²	Electrolyte	Ref.
Gd-NiFe-LDH@CC	210	1 M KOH	This work.
Ce-Ni-Fe-LDH	242	1 M KOH	[11]
NiFeCr/NF	240	1 M KOH	[12]
^s Au/NiFe LDH	237	1 M KOH	[13]
MnO _x /NiFe-LDHs	216	1 M KOH	[14]
NiFeCe-LDH/CNT	227	1 M KOH	[15]
NiFeCe-LDH/MXene	260	1 M KOH	[16]
NiFe-LDH	348	0.1 M KOH	[17]
NiFeCo-LDH/CF	249	1 M KOH	[18]
IrO ₂ @SL-NiFe LDHs	274	1 M KOH	[19]
Co(OH) ₂ /CNTs-IrCl _x	230	1 M KOH	[20]
Co-Mac-1	320	1 M KOH	[21]
NiFe/NiFe-OH	222	1 M KOH	[22]
Ir/Ni(OH) ₂	224	1 M KOH	[23]
NiTe@NiFe-LDH	218	1 M KOH	[24]
NiFeCr LDH	280	1 M KOH	[25]
PM-NiFe-LDH	230	1 M KOH	[26]
NiFeRu-LDH	225	1 M KOH	[27]

Table S3. Yield O₂ volume during Faradic efficiency (FE) test process.

Time / min	$V_{measured}$ / mL	$V_{calculated}$ / mL	FE / %
0-10	0.70	0.76	92.10
10-20	0.74	0.76	97.36
20-30	0.73	0.76	96.05
30-40	0.77	0.76	101.3
40-50	0.75	0.76	98.68
50-60	0.73	0.76	96.05

References

- [1] S. Grimme, J. Antony, S. Ehrlich, H. Krieg, *J. Chem. Phys.* **2010**, 132, 154104.
- [2] X. Fu, B. Warot-Fonrose, R. Arras, D. Demaille, M. Eddrief, V. Etgens, V. Serin, *Appl. Phys. Lett.* **2015**, 107, 062402.
- [3] W. Kohn, L. J. Sham, *Phys. Rev.* **1965**, 140, A1133.
- [4] H. J. Monkhorst, J. D. Pack, *Phys. Rev. B* **1976**, 13, 5188.
- [5] O. Vinogradova, D. Krishnamurthy, V. Pande, V. Viswanathan, *Langmuir* **2018**, 34, 12259.
- [6] J. K. Nørskov, J. Rossmeisl, A. Logadottir, L. Lindqvist, J. R. Kitchin, T. Bligaard, H. Jonsson, *J. Phys. Chem. B* **2004**, 108, 17886.
- [7] I. C. Man, H. Y. Su, F. Calle - Vallejo, H. A. Hansen, J. I. Martinez, N. G. Inoglu, J. Kitchin, T. F. Jaramillo, J. K. Nørskov, J. Rossmeisl, *ChemCatChem* **2011**, 3, 1159.
- [8] M. Bajdich, M. García-Mota, A. Vojvodic, J. K. Nørskov, A. T. Bell, *J. Am. Chem. Soc.* **2013**, 135, 13521.
- [9] J. Behler, *J. Chem. Phys.* **2011**, 134, 074106.
- [10] M. Bajdich, M. Garcia-Mota, A. Vojvodic, J. K. Nørskov, A. T. Bell, *J. Am. Chem. Soc.* **2013**, 135, 13521.
- [11] H. Xu, C. Shan, X. Wu, M. Sun, B. Huang, Y. Tang, C.-H. Yan, *Energy Environ. Sci.* **2020**, 13, 2949-2956.
- [12] X. Bo, R. K. Hocking, S. Zhou, Y. Li, X. Chen, J. Zhuang, Y. Du, C. Zhao, *Energy Environ. Sci.* **2020**, 13, 4225-4237.
- [13] J. Zhang, J. Liu, L. Xi, Y. Yu, N. Chen, S. Sun, W. Wang, K. M. Lange, B. Zhang, *J. Am. Chem. Soc.* **2018**, 140, 3876.
- [14] Y. Xue, Z. S. Fishman, J. A. Röhr, Z. Pan, Y. Wang, C. Zhang, S. Zheng, Y. Zhang, S. Hu, *J. Mater. Chem. A* **2018**, 6, 21918.
- [15] H. Xu, B. Wang, C. Shan, P. Xi, W. Liu, Y. Tang, *ACS Appl. Mater. Interfaces* **2018**, 10, 6336.
- [16] Y. Wen, Z. Wei, J. Liu, R. Li, P. Wang, B. Zhou, X. Zhang, J. Li, Z. Li, *J. Energy Chem.* **2021**, 52, 412.
- [17] F. Dionigi, Z. Zeng, I. Sinev, T. Merzdorf, S. Deshpande, M. B. Lopez, S. Kunze, I. Zegkinoglou, H. Sarodnik, D. Fan, A. Bergmann, J. Drnec, J. F. Araujo, M. Gliech, D. Teschner, J. Zhu, W. X. Li, J. Greeley, B. R. Cuenya, P. Strasser, *Nat. Commun.* **2020**, 11, 2522.
- [18] Y. Lin, H. Wang, C. K. Peng, L. Bu, C. L. Chiang, K. Tian, Y. Zhao, J. Zhao, Y. G. Lin, J. M. Lee, L. Gao, *Small* **2020**, 16, 2002426.
- [19] D. Li, T. Li, G. Hao, W. Guo, S. Chen, G. Liu, J. Li, Q. Zhao, *Chem. Eng. J.* **2020**, 399.
- [20] Y. Huang, G. Wei, J. He, C. An, M. Hu, M. Shu, J. Zhu, S. Yao, W. Xi, R. Si, Z.-M. Zhang, C. An, *Appl. Catal. B: Environ.* **2020**, 279, 119398.
- [21] Q. Liu, Q. Wang, J. Wang, Z. Li, J. Liu, X. Sun, J. Li, Y. Lei, L. Dai, P. Wang, *Adv. Funct. Mater.* **2020**, 30, 2000593.

- [22] W. Zhu, W. Chen, H. Yu, Y. Zeng, F. Ming, H. Liang, Z. Wang, *Appl. Catal. B: Environ.* **2020**, 278, 119326.
- [23] G. Zhao, P. Li, N. Cheng, S. X. Dou, W. Sun, *Adv. Mater.* **2020**, 32, 2000872.
- [24] H. Sun, J.-M. Yang, J.-G. Li, Z. Li, X. Ao, Y.-Z. Liu, Y. Zhang, Y. Li, C. Wang, J. Tang, *Appl. Catal. B-Environ.* **2020**, 272.
- [25] Y. Yang, L. Dang, M. J. Shearer, H. Sheng, W. Li, J. Chen, P. Xiao, Y. Zhang, R. J. Hamers, S. Jin, *Adv. Energy Mater.* **2018**, 8, 1703189.
- [26] X. Zhang, Y. Zhao, Y. Zhao, R. Shi, G. I. N. Waterhouse, T. Zhang, *Adv. Energy Mater.* **2019**, 9, 1900881.
- [27] G. Chen, T. Wang, J. Zhang, P. Liu, H. Sun, X. Zhuang, M. Chen, X. Feng, *Adv. Mater.* **2018**, 30, 1706279.